

The Fracture Energy of Bimaterial Interfaces

A.G. EVANS, M. RÜHLE, B.J. DALGLEISH, and P.G. CHARALAMBIDES

This article describes a framework applicable to the measurement and interpretation of the fracture energy of bimaterial interfaces. A major conclusion of this study is that the fracture energy, Γ_i , is not unique and usually exhibits values substantially larger than the thermodynamic "work of adhesion." The lack of uniqueness is related to mode mixity (shear/opening) effects experienced by interface cracks, as characterized by the phase angle of loading, ψ : typically, Γ_i is found to increase as ψ increases. These trends are attributed to crack shielding caused by roughness of the interface fracture surface, to material nonlinearity, *etc.* The phase angle is, in turn, influenced by the choice of test specimen, resulting in values of Γ_i that differ between specimens in a manner attributed to the locus of Γ_i with ψ . Preliminary models that relate Γ_i to roughness, plasticity, segregation, *etc.*, are described, leading to insights concerning microstructural aspects of "weak" and "strong" interfaces.

I. INTRODUCTION

THE fracture energy of interfaces between dissimilar materials, Γ_i , exerts a critical influence on many problems of technological importance, particularly the mechanical properties of composites^[1,2,3] and the decohesion of films and coatings,^[3-7] as well as the strength of bonds.^[8,9] The specific role of the fracture energy is first outlined for several of these problems, as needed to provide a conceptual framework for studies of Γ_i . Subject to this background and with the adoption of a practicable mechanics formulation for characterizing interface cracks, methods for measuring Γ_i on bimaterial systems of interest are described. Experimental measurements and observations of interface fractures are presented, as well as atomistic, chemical, and microstructural features of typical interfaces. Preliminary attempts are then made to relate Γ_i to the salient characteristics of interfaces, using the appropriate models.

The conceptual framework for addressing the interface fracture energy derives from notions already established for interpreting the fracture energy of brittle solids.^[10,11] The most basic contribution to Γ_i , which often leverages all others, is the work of adhesion, W_{ad} , and the effect on that quantity of segregants at the interface, as given by^[10]

$$\Gamma_0 = W_{ad} - \sum_i (\Delta g_i^\circ - \Delta g_s^\circ) c_i \quad [1]$$

where c_i is the concentration of segregant per unit area of interface and Δg° is the Gibbs free energy of segregation. The subscript i refers to the interface and s to

the free surface. For a planar interface in a system having constituents with linear constitutive characteristics,^[11]

$$\Gamma_i = \xi \Gamma_0 \quad [2]$$

where ξ is a quantity ($1 \leq \xi \leq 10$) which characterizes the nonequilibrium thermodynamic state of the surface created by fracture. Nonlinearity of either constituent and nonplanarity of the interface introduce other *multiplicative* contributions to Γ_i , based on crack shielding and dissipation. The roughness-related shielding is manifest in a parameter,^[12]

$$\chi = EH^2/L\Gamma_0 \quad [3]$$

where H is the amplitude, L is the wavelength of roughness, and E is Young's modulus. Plasticity occurring in one of the bonded layers can cause plastic dissipation, governed by a nondimensional parameter^[13,14]

$$\zeta = E\Gamma_0/Y^2h \quad [4]$$

where Y is the yield strength and h the thickness of the ductile layer. The plastic dissipation is multiplicative with Γ_0 provided that the materials involved have viscoplastic properties that allow a strong singularity to be retained at the crack tip.^[10,15] Otherwise, the crack tip blunts, and there is no energy release through the crack tip, resulting in a mechanism of interface fracture that may be insensitive to W_{ad} .

The measured fracture energy thus typically incorporates several contributions, each of which must be evaluated and understood in order to control the mechanical behavior of interfaces in composites, coatings, bonds, *etc.* The intent of the present article is to provide an assessment of the present status of this topic.

One of the important principles established by recent research is that *shear* (mode II) displacements experienced by an interface crack have an important influence on the interface fracture process.^[12] Indeed, such displacements can influence the magnitude of Γ_i and determine whether the crack either remains at the interface or propagates into one of the adjoining materials.^[16] A quantity that contains the salient information about the shear displacements is the phase angle of loading, ψ ,^[17]

A.G. EVANS, Professor, is with the Materials Department, University of California, Santa Barbara, CA 93106. M. RÜHLE is with the Max Planck Institut für Metallforschung, Stuttgart, Federal Republic of Germany. B.J. DALGLEISH is with Materials Development, Berkeley Laboratory, Berkeley, CA. P.G. CHARALAMBIDES is with the Department of Mechanical Engineering, Michigan State University, East Lansing, MI.

This paper is based on a presentation made in the symposium "Interface Science and Engineering" presented during the 1988 World Materials Congress and the TMS Fall Meeting, Chicago, IL, September 26-29, 1988, under the auspices of the ASM-MSD Surfaces and Interfaces Committee and the TMS Electronic Device Materials Committee.

which is a measure of the relative shear to opening experienced by the interface crack surfaces near the tip. The angular range of interest is

$$-\pi/2 < \psi < \pi/2$$

The bounds at both $\pi/2$ and $-\pi/2$ represent interface cracks having zero opening, whereas $\psi = 0$ refers to a crack with zero shear. Typically, Γ_i is found to increase as ψ deviates from zero, as schematically depicted in Figure 1, primarily because of the influence of the relative shearing of the crack surface on shielding, dissipation, etc.

Another topic considered within the above framework is the distinction between "chemical" and "mechanical" bonding. The latter has had an ambiguous significance in the bonding literature, seemingly because mechanical effects become more pronounced as ψ increases. The relative chemical and mechanical contributions to Γ_i are addressed as these issues emerge.

II. THE MECHANICS OF INTERFACE CRACKS

A. Basic Principles

Cracks at bimaterial interfaces exhibit crack tip characteristics that have been the subject of extensive debate in the mechanics literature, and this debate still continues.^[17,18] In the absence of a consensus concerning the appropriate mechanics, an approach has been suggested^[17,19] whereby simplifying hypotheses can be made. Based on these hypotheses, tests can be designed and fracture energy data obtained. Uniqueness of the data, when established, provides validation of the approach.

The bimaterial elastic properties that govern plane strain interface crack fields are the Dundurs' parameters,^{[20]*}

*Consistent with published articles by Hutchinson and colleagues, the Dundurs' parameters used here are the negative of those given in Eq. [5].

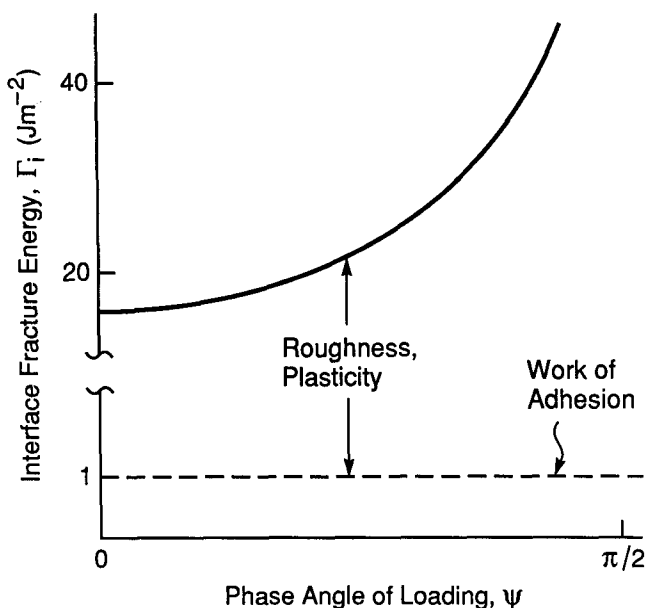


Fig. 1—A schematic illustration of a typical trend in the interface fracture energy, Γ_i , with the phase angle of loading, ψ .

$$\alpha = \frac{\mu_1(1 - \nu_2) - \mu_2(1 - \nu_1)}{[\mu_1(1 - \nu_2) + \mu_2(1 - \nu_1)]}$$

$$\beta = \frac{\mu_1(1 - 2\nu_2) - \mu_2(1 - 2\nu_1)}{2[\mu_1(1 - \nu_2) + \mu_2(1 - \nu_1)]} \quad [5]$$

and a related parameter, $\varepsilon = (1/2\pi) \ln [(1 - \beta)/(1 + \beta)]$. In the above expressions, μ is the shear modulus, ν the Poisson's ratio, and the subscripts 1 and 2 refer to the two materials. Nonzero values of β cause the crack tip stress and displacement fields to oscillate,^[17] leading to crack surface interpenetration. Such interpenetration introduces evident ambiguity into the characteristics of interface fracture. However, it has been recognized that for many bimaterial systems of interest, β is small^[5,21] (Figure 2). It has thus been proposed that a zero β hypothesis should provide an adequate interface fracture characterization in many cases. With this hypothesis, the familiar square root singularity is retained at the crack tip, and fracture can be expressed in terms of two parameters. The *first parameter* is the familiar fracture energy, Γ_i , which can be evaluated based on an energy release rate, \mathcal{G} , calibration of test specimens. In many cases, \mathcal{G} can be determined analytically from straightforward strain energy considerations.^[3,22,24] In other instances, \mathcal{G} is directly related to the crack surface displacements, u and v (Figure 3):^[17]

$$\mathcal{G} = \frac{\pi(u^2 + v^2)(1 + 4\varepsilon^2)}{8[(1 - \nu_1)/\mu_1 + (1 - \nu_2)/\mu_2]} \quad [6]$$

whereupon solutions for \mathcal{G} may be obtained within a finite element scheme.^[23] Such solutions are presented below for a variety of useful test specimens and interface decohesion problems.

The second important parameter is the phase angle of loading, ψ , which is a measure of the *mixture of shear to opening* experienced by the interface crack surface. An expression for ψ when $\beta = 0$ is

$$\psi = \tan^{-1}(v/u) \quad [7]$$

indicating that ψ can be determined either from finite element calculations^[24] or by using integral equation

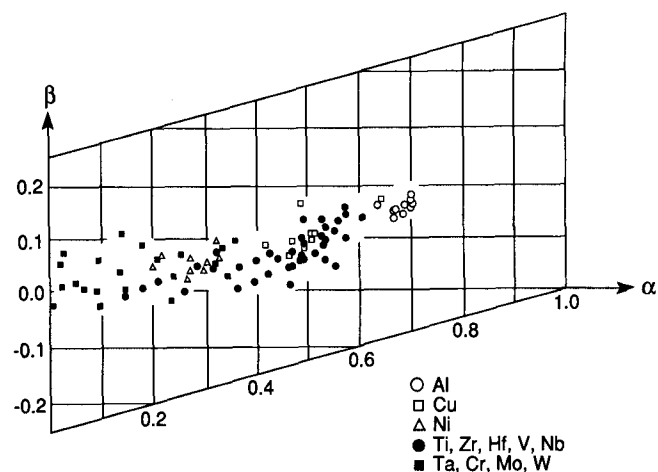


Fig. 2—Bimaterial interfaces of interest plotted in α, β space.^[21] The symbols refer to the metal member bonded to a range of different ceramics.

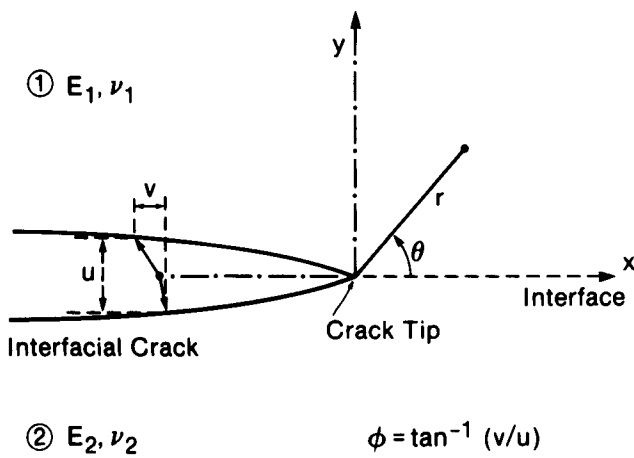


Fig. 3—A crack on a bimaterial interface indicating the relative shear to opening displacements experienced by the crack surfaces.

methods.^[5,16] In either case, determination of ψ is non-trivial. Consequently, ψ has not been as broadly evaluated as \mathcal{G} for the test configurations and debonding problems of interest. Yet, as already noted and further elaborated below, the sign and magnitude of ψ have several profound implications for interface fracture.

One important feature of bimaterial interface cracks which should be emphasized is that ψ is often nonzero even when the external loading is normal to the interface plane.^[17] This situation arises because of the elastic mismatch across the interface. Furthermore, the magnitude of ψ may be a function of crack length. Consequently, when solving interface fracture problems, it is *essential* that ψ be calculated. This feature of interface fracture represents the major difference from the familiar treatment of fracture within an elastically homogeneous medium.

An interface fracture configuration frequently used for testing and often encountered in debonding problems involves a thin sandwich layer (Figure 4(a)) within an otherwise elastically homogeneous system. For this case, when the layer thickness h is small compared with all other dimensions (specimen size, crack length, *etc.*), the energy release rate is the same as that evaluated for the homogeneous case. However, the phase angle ψ rotates.^[25] The rotation is strictly dictated by the Dundurs' parameters (α, β), as they govern the elastic mismatch between the sandwich layer material and the adjoining material. Furthermore, when $\beta \approx 0$, the rotation angle ω is a simple function of α (Figure 4(b)). This phase angle "correction" can be used for any sandwich specimen configuration, provided that h is small.

B. Crack Path Considerations

In elastically homogeneous brittle solids, cracks have been found to follow a local trajectory for which $K_{II} = 0$.^[5,22,26] An important corollary of this observation is that cracks for which $K_{II} \neq 0$ (*i.e.*, $\psi \neq 0$) deflect out of their existing planes until the $K_{II} = 0$ condition is satisfied. However, cracks at interfaces are not limited by this criterion because the bimaterial system has

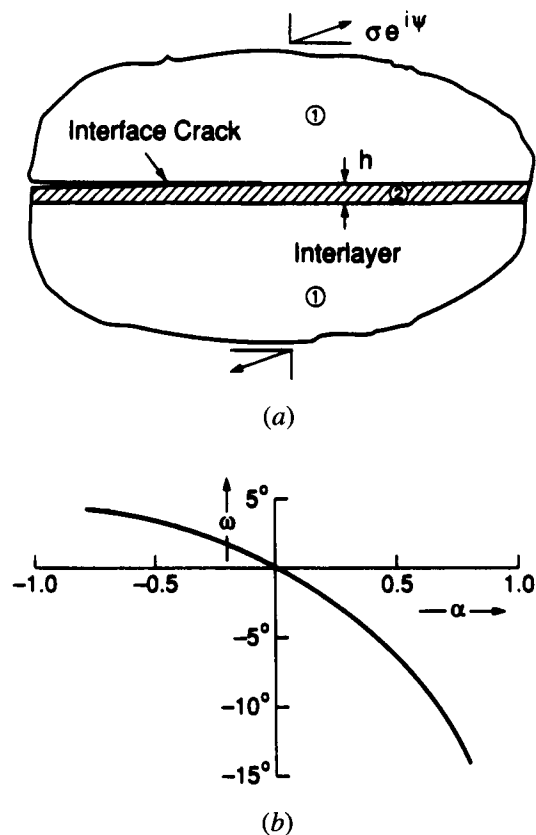


Fig. 4—(a) A crack on one interface in a sandwich layer system and (b) the phase angle of rotation, ω , caused by a thin sandwich layer.

inhomogeneous fracture energy: specifically, one value for the interface $\Gamma_i(\psi)$ and other values for each constituent material, Γ_1 and Γ_2 . Consequently, when Γ_i is relatively small, the crack can extend along the interface, even when $\psi \neq 0$. Indeed, the range of relative fracture energies that allow cracks to remain at the interface has been calculated^[16] as a function of ψ for the interface crack (Figure 5). The sign of ψ is of particular significance in this regard, and consequently, for convenience, a sign convention is selected wherein positive ψ tends to deflect the crack into the ceramic and *vice versa*.

When the crack is trapped at the interface, Γ_i can be measured as a function of ψ , as elaborated below. Otherwise, when ψ is positive, the crack moves out of the interface, and then the measured fracture energy refers to the adjoining ceramic material. It is also apparent from Figure 5(a) that cracks located at the interface when ψ is small and positive can deflect away from the interface should ψ become large. Since the sign and magnitude of ψ are strongly influenced by the choice of test specimen, the observed crack path can also be specimen geometry-dependent. Finally, it is noted that when ψ is negative, the crack tends to deflect into the metal, but such deflection cannot occur and, instead, the crack remains at the interface, often detaching ceramic "chips" at flaws that preexist in the ceramic near the interface (Figures 5(b) and (c)). In this case, interface crack propagation has ample opportunity to induce plastic deformation in the metal.

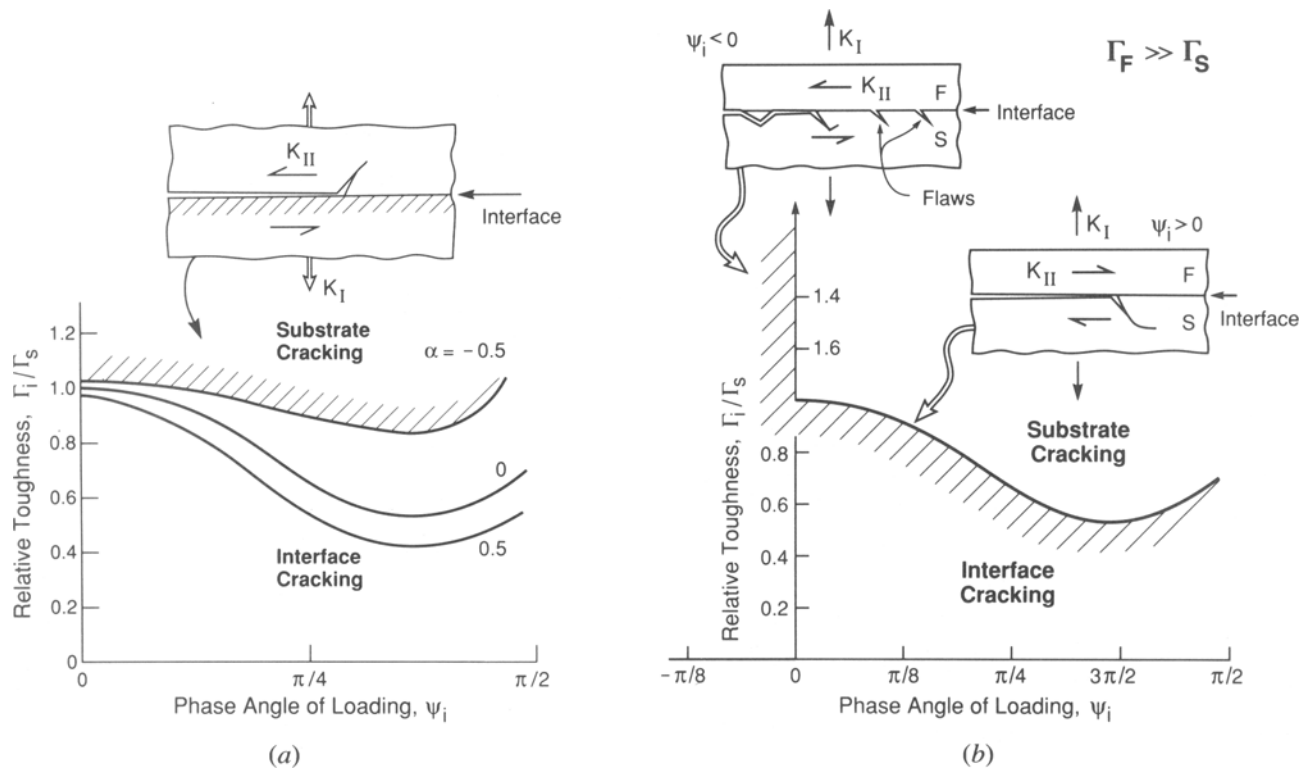


Fig. 5—Crack path diagram for interface cracks: (a) at positive ψ for three values of α (with $\beta = 0$), (b) a metal/ceramic interface indicating the expected behavior at negative ψ , and (c) an alumina chip attached to a fracture surface with gold.

III. SOME IMPORTANT INTERFACE FRACTURE PROBLEMS

A. Film Decohesion

Residually stressed thin films can decohere from substrates by fracturing along the interface. This process is governed by a nondimensional parameter,^[27]

$$\Omega = E_f \Gamma_i / \sigma^2 h \quad [8]$$

where σ is the stress in the film and h is the film thickness. Specifically, film decohesion along the interface is prohibited when Ω is less than a critical value Ω_c , leading to the definition of a critical film thickness, h_c , below which *decohesion cannot occur*,

$$h_c = E_f \Gamma_i / \sigma^2 \Omega_c \quad [9]$$

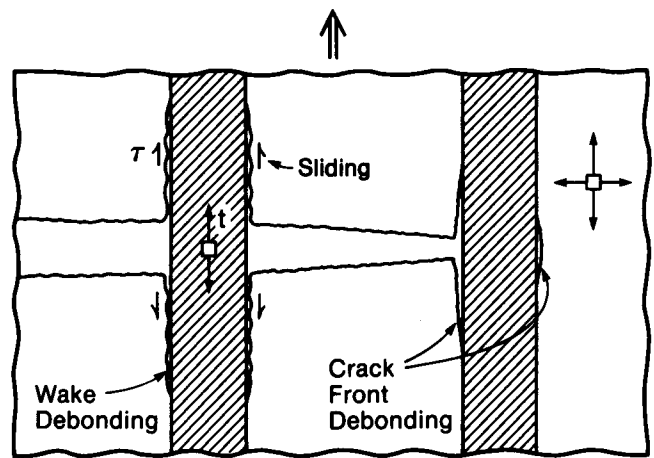
While Ω_c is dependent on the elastic mismatch α and on the sign of the residual stress, as well as the substrate

yield strength, its magnitude is typically of order unity^[27] (Figure 6).

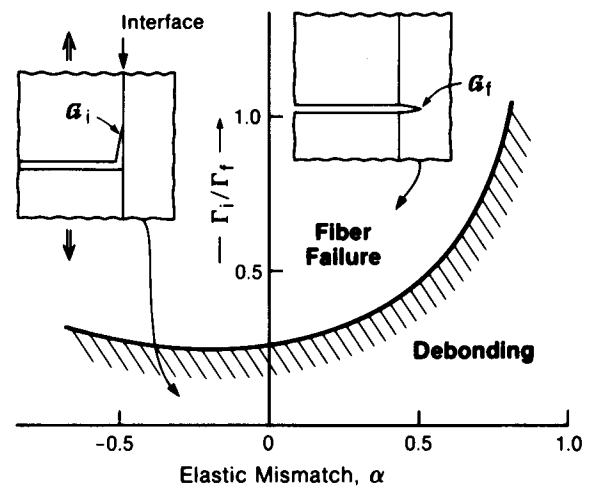
The importance of the interface fracture energy to decohesion, evident from Eq. [9], is qualified by its dependence on the phase angle ψ . The sign and magnitude of ψ depends on the sign of the residual stress in the film (tension or compression) and the mode of delamination. For films in tension, delamination occurs from edges, holes, or splits in the film,^[4,5,27] and in all cases, ψ is of order 50 deg (for $\beta = 0$). For films in compression, edge decohesion occurs with $\psi = 90$ deg (i.e., a strictly mode II/III process), whereas buckling-induced decohesion occurs for ψ in the range of 0 to ~ 50 deg, depending on the interface crack radius.^[6] Thus, the prediction of the critical film thickness using Eq. [9] in general, requires that Γ_i be known over a wide range of ψ .

B. Debonding in Brittle Matrix Composites

Fiber reinforcement of brittle matrices (ceramics and/or intermetallics) leading to high toughness can only be accomplished if debonding between matrix and fiber occurs at the crack front^[1,2] (Figure 7(a)). Such debonding requires that the ratio Γ_i/Γ_f , where Γ_f is the mode I fracture energy of the fiber, be small^[16] (< 0.25 , Figure 7(b)). Furthermore, the phase angle associated with the debonding process is of order 45 deg (Figure 7(b)). Consequently, a prerequisite for high toughness in brittle matrix composites is that Γ_i/Γ_f satisfy the debonding requirement of Figure 7, with Γ_i being evaluated at $\psi \approx 45$ deg. Following crack front debonding, further debonding is typically required in the crack wake^[1,28] (Figure 7(a)). In this case, the extent of debonding is governed by Γ_i at large values of ψ ($\rightarrow 90$ deg). Furthermore, the specific phase angle needed to address wake debonding is sensitive to the residual strain. Compressive residual strain normal to the interface gives values of $\psi \approx 90$ deg and causes stable debonding. Conversely, tensile residual strain encompasses the range -50 deg $< \psi < 70$ deg. Again, therefore, knowledge



(a)



(b)

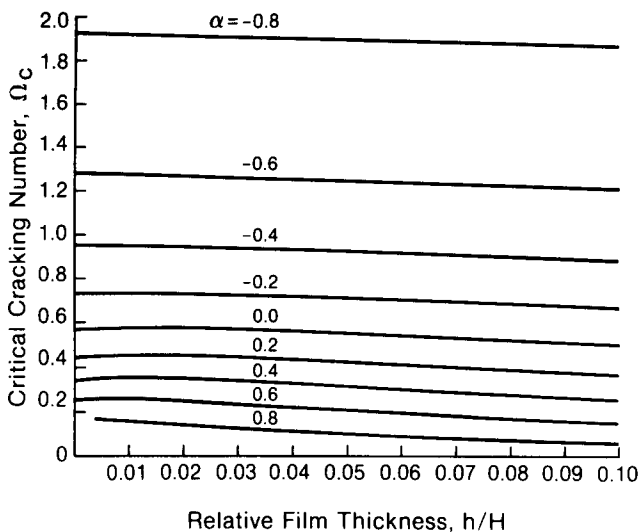


Fig. 6—Trends in decohesion number for films on a brittle substrate.

Fig. 7—(a) A schematic illustrating crack front debonding in fiber-reinforced brittle materials and (b) a crack front debond diagram.

of Γ_i over a wide range of phase angles is needed to understand debonding in composites.

C. The Strength of Bonds

The strength of bonded systems is typically dominated by flaws that exist near the edge in the vicinity of the

bonded interface^[8,9] (Figure 8). Specifically, the strength, S , of a bond when fracture occurs at the interface is related to the fracture energy by^[17]

$$S^2 = \frac{16\Gamma_i(\psi)}{(1 + \lambda)\pi a(c_1 + c_2)^2} \quad [10]$$

where λ is a measure of the stress concentration caused by mechanical property mismatch across the interface and by thermal expansion mismatch,^[8,9] a is the radius of flaws located at the interface (Figure 8), and ψ (when $\beta \cong 0$) is the same as that for the actual interface stresses at the location of the flaw. The term c is equal to $(\kappa + 1)/\mu$, with $\kappa = 3 - 4\nu$ for plane strain, and the subscripts 1 and 2 refer to the material on either side of the interface. The connection between Γ_i and S thus involves knowledge of interface flaws, as well as of property mismatches and of configurational effects. In particular, when the bond material has the higher thermal expansion, the phase angle at interface edge flaws associated with the residual field is $\psi = 90$ deg, often resulting in fractures that deviate away from the interface.^[8,29] Conversely, low expansion bond materials give $\psi \approx 45$ deg at interface flaws and tend to encourage fracture at the interface.^[8,29] However, upon loading, ψ changes such that the magnitude of Γ_i that governs bond failure may also change. The functional dependence of Γ_i on ψ , as well as flaw size statistics,^[9] should thus be known in order to predict and interpret bond strengths.

IV. TEST METHODS

A variety of specimens capable of providing measurements of the interface fracture energy Γ_i now exists. Some of the most extensively used techniques are summarized schematically in Figure 9, with the phase angle range typical of each specimen and the associated energy release rate also indicated. Several important factors arise concerning method selection when consideration is given to issues such as creating and measuring sharp precracks

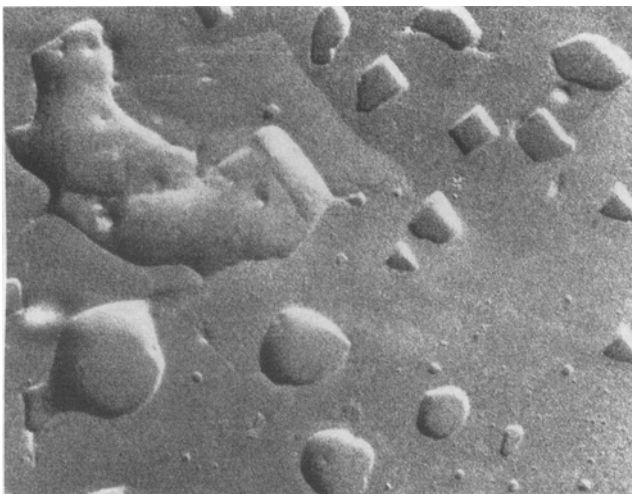


Fig. 8—Flaws at a Au/Al₂O₃ interface associated with incomplete diffusion bonding.

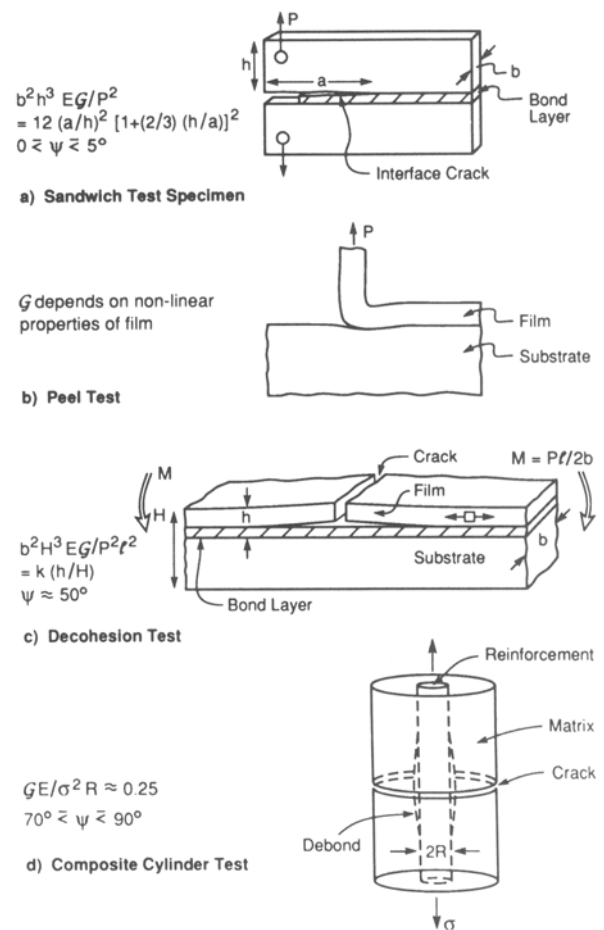


Fig. 9—Some typical test specimens used to measure the interface fracture energy.

at the interface, as well as the nonuniqueness of Γ_i , which dictates that Γ_i be measured over the phase angle range of practical significance.

Precracking facility, followed by accurate determination of Γ_i and ψ , is enhanced by selecting test specimens that provide significant interface regions in which steady state obtains: Γ_i and ψ independent of crack length. The delamination,^[24] peel,^[30] and pull-out specimens^[28] each exhibit steady-state regions, albeit with different phase angles. The peel specimen has the disadvantage that a full nonlinear description of the film material is needed to evaluate Γ_i .^[30] The pull-out specimen has the disadvantage that it is difficult to fabricate, and furthermore, \mathcal{G} , as well as ψ , is sensitive to residual strain caused by thermal expansion mismatch between the two materials.^[28] Consequently, the delamination sandwich specimen^[24] is deemed the most useful for initial investigation of fracture energy trends at interfaces of practical interest.

A full understanding of the fracture energy of a particular interface normally requires that several different specimens be used,^[31] each capable of carefully exploring a specific range of phase angles. With this background, each of the test specimens depicted in Figure 9 is discussed, with emphasis on the $\mathcal{G}(\psi)$ calibration, including the influence of residual strain. Fracture energies of several bimaterial pairs are listed in Table I.

A. Delamination Specimen

Sandwich test specimens amenable to delamination testing can be readily made either by the diffusion bonding or adhesive bonding of plates,^[24,32,33] followed by the use of standard cutting and grinding procedures to create beams ready for testing. Precracking can also be routinely achieved by emplacing a Knoop indentation into the center of the beam and loading in three-point bending, with the indentation at the location of maximum tension. The indentation crack propagates across the lower layer up to the interface, and when $\Gamma_i \approx 4 \Gamma_s$, the precrack continues extending along the interface to a distance of the order of the layer thickness, h . When precracked in this way, the specimen can be tested either in four-point flexure or in uniaxial tension. Usually the former is preferred, because specimen alignment problems are readily addressed and because the inherently stiff loading system allows superior control of crack propagation.

Analysis of the four-point flexure delamination specimen has indicated that \mathcal{G} can be expressed in the nondimensional form^[24]

$$\frac{\mathcal{G} E_2 b^2 H^3}{P^2 l^2 (1 - \nu^2)} = F\left(\frac{a}{l}, \alpha, \frac{h}{H}\right) \quad [11]$$

where P is the imposed load, l is the moment span (Figure 9), b is the specimen width, H is the total thickness, h is the thickness of the outer layer, a is the crack length, and F is a function. The preferred testing configuration has $h \ll H$ and consists of a thin sandwich layer, with the interface crack front in the steady-state region between the inner loading lines (spacing $2c$). Then, Eq. [11] simplifies to a function of h/H only, as plotted in Figure 10. The corresponding phase angle (for $\beta \approx 0$) is

$$\psi = \phi + \omega$$

where ϕ is in the range of 42 to 49 deg, depending upon h/H and ω , as plotted in Figure 4(b). For specimen di-

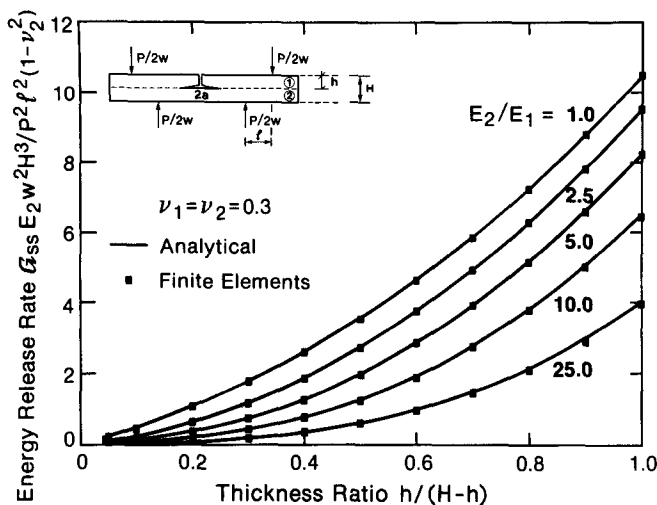


Fig. 10—Trend in the nondimensional steady-state energy release rate with relative beam thickness for the delamination specimen. The elastic modulus ratio E_2/E_1 is related to the Dundurs' parameter by $E_2/E_1 = (1 - \alpha)/(1 + \alpha)$ for $\nu_1 = \nu_2$.

mensions in the range of $0.05 \approx h/H \approx 0.5$, steady-state behavior essentially obtains for interface cracks in the extensive crack length range, $0.2h \approx a \approx 0.9c$, where $2c$ is the inner span.

When conducting four-point flexure delamination tests, a practical issue concerns friction at the loading points. Experience has indicated that friction is difficult to eliminate. However, the effects of friction can be taken into account by measuring the compliance hysteresis.^[34] Specifically, by loading and unloading the specimen to loads below the critical crack growth load, friction is manifest as a differential in compliance, evident in measurements of the centerpoint displacement, u . Finally, it is noted that when a bimaterial beam is used, rather than a sandwich specimen, residual stresses typically exert an important influence on \mathcal{G} and on ψ .^[34] These effects have been calculated and "corrections" to \mathcal{G} , which allow explicit determination of Γ_i , can be implemented, provided that the misfit stress has been independently measured.

B. The Composite Cylinder

Fracture energies obtained from composite cylinder tests (Figure 9) have direct relevance to interface debonding problems in composites (Figure 7). However, test specimens are difficult to produce and the test results equally difficult to interpret. Test specimens have been made by hot isostatic pressing, by melt processing, and by adhesive bonding, but rigorous relationships between $\mathcal{G}(\psi)$ and the experimental variables accessible during testing exist for only a limited set of bimaterial interfaces. Specifically, when the residual stress normal to the interface is tensile^[28] and the debond surfaces are sufficiently smooth that the crack surface contact zone is small compared with the debond length, d , a steady-state debonding condition has been identified. Steady state is established when $d \approx R$ (the "fiber" radius) such that \mathcal{G} has the form^[28]

$$\frac{\mathcal{G}}{E_f R e^2} = \kappa_1 + \kappa_2 \tau + \kappa_3 \tau^2 \quad [12]$$

where $\tau = t/E_f e$, with t being the applied stress on the fiber, e the misfit strain, and $\kappa_i, i = 1, 2, 3$ coefficients that depend on the elastic mismatch, α (Table II), and the relative "fiber" volume, f . The phase angle of loading is typically large and depends somewhat on α (Figure 11).

C. The Peel Test

The peel test has practical utility for thin flexible films on substrates.^[30] For such cases, most of the metal and polymer films of interest undergo nonlinear deformation. This deformation provides a major contribution to the work done by the steady-state peel force, P_s , and this work needs to be quantified in order to use P_s to evaluate Γ_i . The magnitudes of the plastic dissipation and of the residual strain energy in the film have been calculated, allowing Γ_i to be deduced, provided that the nonlinear constitutive properties of the film material are known. It is also apparent that ψ is negative. The negative sign of the phase angle has the implication that for ductile/tough

Table I. Fracture Energy of Bimaterial Interfaces

Bimaterial Pairs	Phase Angle	Γ_i (Jm ⁻²)	Test Method
Silica/polymer ^[31]	5 deg	7	double cantilever beam cylinder
	70 deg	20	
Al ₂ O ₃ /glass ^[40]	0 to 1 deg	8 ± 1	bend delamination
	50 deg	8 ± 1	
SiC/Si ^[7]	—	5.5	thin film buckling
Cu/Si ^[30]	—	5.5	peel
Cu/glass ^[35]	5 deg	1 – 10	double cantilever beam
Au/sapphire ^[36] (0001)	50 deg	>20	delamination
Pt/sapphire* (0001)	50 deg	40 ± 4	delamination
Cu(Cr)/polyimide ^[30]	—	200 ± 30	peel
Nb/Al ₂ O ₃	-5 deg	80 ± 30	notch bend

Table II. Energy Release Rate Parameters for Residually Stressed Composites ($f = 0.2$)

α	k_1	k_2	k_3
0.3	0.189	-0.280	0.152
0.0	0.314	-0.370	0.200
-0.3	1.486	-0.430	0.228

films, the debond crack is induced to propagate within the interface rather than extend into the substrate. Interface debonding is thus observed even when the interface fracture energy Γ_i is well in excess of that for the substrate (Figure 5).

The above behavior can be modified when appreciable residual stress preexists within the film, especially when the residual force is of the same order as the peel force. Specifically, the residual stress contributes directly to the steady-state energy release rate and modifies the phase angle of loading. The energy release rate is enhanced by both tensile and compressive residual stress, but the negative phase angle caused by peeling is reduced by residual tension and enhanced by residual compression.

D. Other Methods

Conventional testing procedures, such as compact tension tests (Figure 9) and bend tests, can be used to obtain information about Γ_i at $\psi \approx 0$ if a thin sandwich configuration is adopted.^[35] Then, as already noted, \mathcal{G} is the same as that for the elastically homogeneous material, and ψ is rotated by ω (Figure 4). However, it is emphasized that an effective precracking approach and a method capable of *in situ* crack length measurements are needed to obtain valid measurements of Γ_i .

V. FRACTURE ENERGY DATA

There are relatively few unqualified measurements of the fracture energy of bimaterial interfaces wherein effects on $\mathcal{G}(\psi)$ of residual stress, friction, *etc.*, have been rigorously analyzed. Consequently, a general picture of

trends in Γ_i with the structure and “microstructure” of the interface does not yet exist. Values of Γ_i deemed to be reasonably rigorous are summarized in Table II. The only material system which has been studied over a considerable range of phase angles is a model “elastic” system consisting of glass bonded with polymer.^[31] This system exhibits a fracture energy that increases as ψ approaches $\pi/2$. The trend in Γ_i with ψ has been tentatively attributed to roughness effects as elaborated in the following section.

Some results obtained for three ductile/brittle bonded systems are insightful regarding the role of plasticity. Specifically, for two systems, Cu/glass^[35] and Au/sapphire,^[36] Γ_i is large (~ 10 to 20 Jm⁻², Table II) compared with the work of adhesion, and furthermore, interface fracture involves crack blunting and bridging of the crack surface by ligaments of ductile material (Figure 12). The latter is indicative of a crack shielding contribution to Γ_i . The studies on the latter system also reveal a paradox. Specifically, slip in the metal, evident in the form of slip steps on the crack surface, seemingly causes crack blunting; nevertheless, brittle interface crack extension still occurs.

The third system of interest of Al/Al₂O₃. Fracture in this system *never occurs along the interface*,^[32] indicating that Γ_i exceeds the fracture energy of the constituent materials. Instead, fracture occurs in the Al₂O₃ (Figure 13(a)) when the yield strength of the Al alloy is high and the Al layer is thin, resulting in a fracture energy essentially the same as that for Al₂O₃. Alternatively, when the Al is relatively soft, the Al fractures by a classic ductile dimple mechanism (Figure 13(b)). In the latter case, the interface nevertheless influences the measured fracture energy by acting as a site for hole nucleation (Figure 13(b)), such that the process may be regarded as a *ductile interface fracture process*.

Finally, a significant body of knowledge is available on the Nb/Al₂O₃ system.^[33,37,38] For this system, the interface fracture energies have been estimated using sandwich specimens in bending, with a phase angle of about -5 deg. The results, while not rigorously valid, because notches were used rather than precracks, are believed to be of the correct order. The values obtained

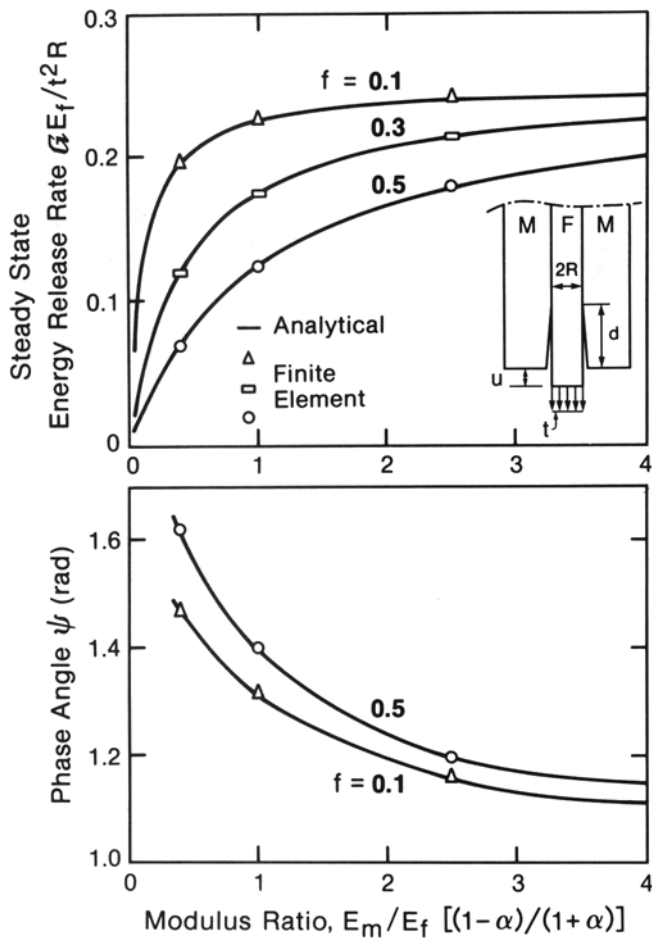


Fig. 11—The nondimensional steady-state energy release rate and phase angle: trends with elastic mismatch and “fiber” volume fraction, f . The modulus ratio E_f/E_m is preferred for axiometric problems, because the Dundurs’ parameters may not uniquely characterize the elastic mismatch.

(Table II) for (0001) sapphire bonded to single crystalline (110) Nb, being in the range of 70 to 110 J/m², are typically larger than the basal plane fracture energy of sapphire Γ_i (≈ 20 Jm⁻²) and much larger than W_{ad} (~ 1 Jm⁻² for this interface). Observations of the inter-

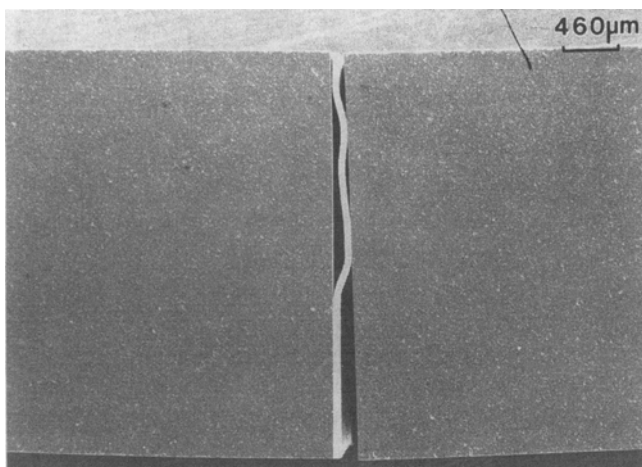
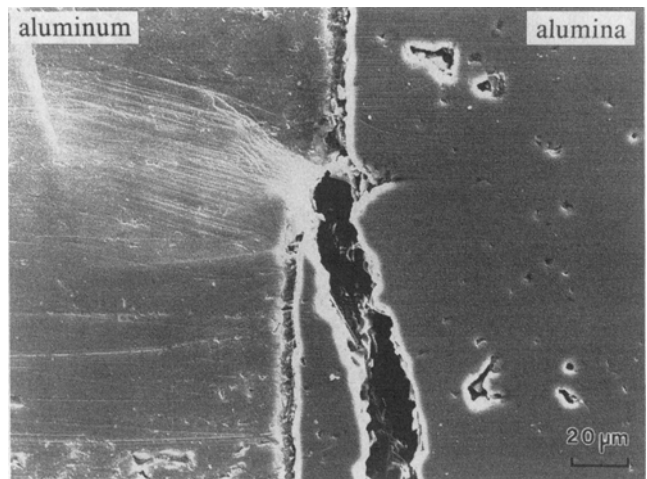
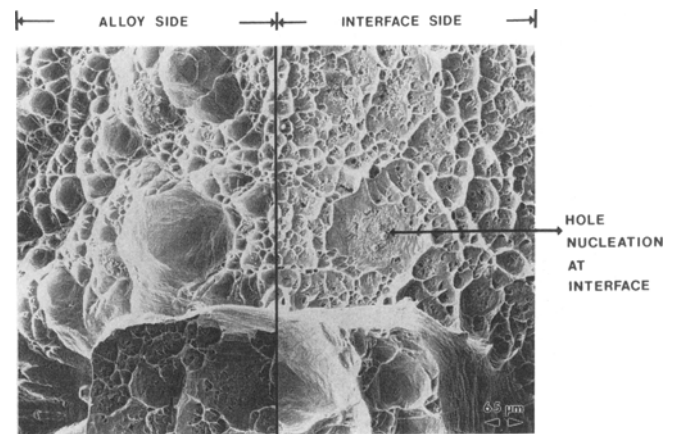


Fig. 12—Crack bridging by Au in a Au/Al₂O₃ sandwich specimen.



(a)



(b)

Fig. 13—The fracture behavior of Al/Al₂O₃ bonds: (a) fracture in the Al₂O₃ near the interface for Al/4 at. pct Mg alloy and (b) matching fracture surfaces for ductile fracture in the Al when “pure” Al is used for bonding.

face (Figure 14) also indicate that it is faceted, but the facet amplitude is small (heights 2.3 to 50 Å). Plastic flow in the Nb is also found to accompany interface fracture, as evident from dislocations observed in the transmission electron microscope (Figure 15). Furthermore, electron backscattering studies in the scanning electron microscope (SEM) have revealed the existence of bands of plasticity in the Nb on (110).

VI. INTERFACE FRACTURE MODELS

Nonplanar interface cracks between two elastic materials are subject to *shielding* by asperity contact^[12] (Figure 16). The length of the contact zone D , and thus the magnitude of the shielding, is governed by the phase angle of loading, ψ , by the parameter χ (Eq. [3]), and by the friction coefficient μ . Specifically, when either ψ or χ are zero, D is zero, and there is no shielding. When both ψ and χ are nonzero, the magnitude of D depends in a coupled manner on ψ , χ , and μ and also on the

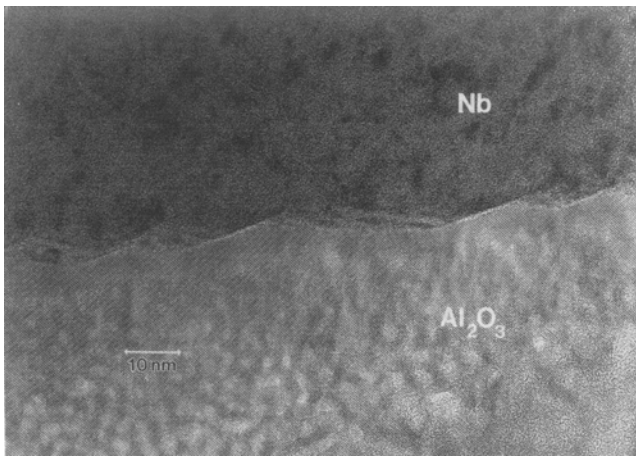


Fig. 14—Interface facets in the Nb/Al₂O₃ interface.

morphology of the roughness. Shielding effects have been calculated for a simple geometric model of the interface and for $\mu = 0$. The results provide useful insight regarding the trends (Figure 16(b)). Two features are of major interest. The shielding effect increases dramatically as $\psi \rightarrow \pi/2$, that is, as the crack opening-to-shear ratio tends to zero (the shear crack limit). In fact, at that limit, contact occurs everywhere along the crack. The shielding is also strongly influenced by the amplitude of the roughness, as manifest in χ . Specifically, when $\chi \approx 10^{-4}$, shielding is only realized when $\psi \approx \pi/2$ and thus has no significant effect on Γ_i over the range in ψ of principal importance. Conversely, when $\chi > 10^{-1}$, the shielding effect saturates such that further increase in roughness amplitude have no additional influence on Γ_i . Roughness-induced shielding is a possible source of the trend in Γ_i with ψ measured for the glass/polymer system^[31] (Table II). Finally, it is noted that the fracture energy at $\psi = 0$ may be regarded as the “chemical” bonding, while the *increment* in Γ_i as ψ increases can be considered as a “mechanical” contribution.

Plastic deformation of the metal undoubtedly provides a major contribution to Γ_i for each of the metal/ceramic systems indicated in Table II. However, adequate models have yet to be developed and await guidance from the

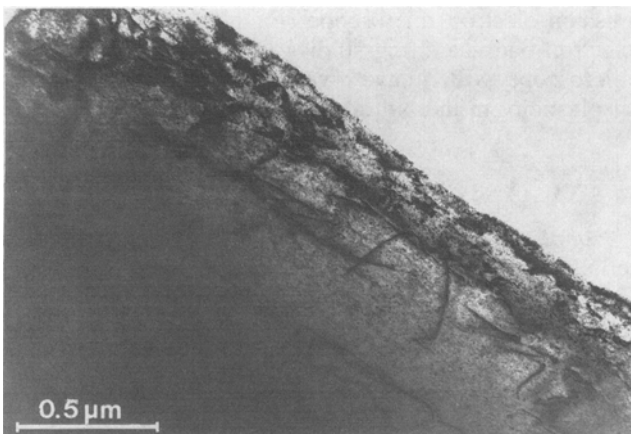
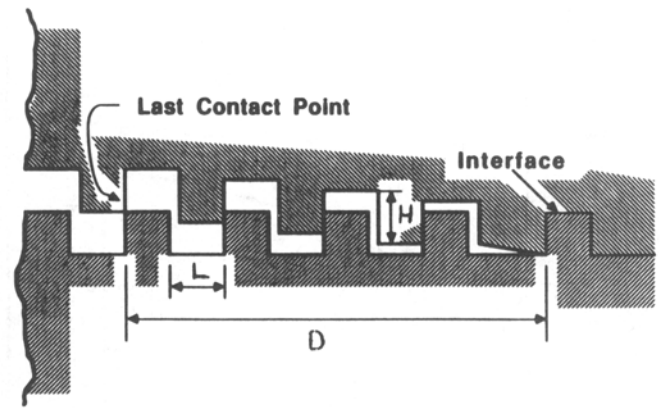
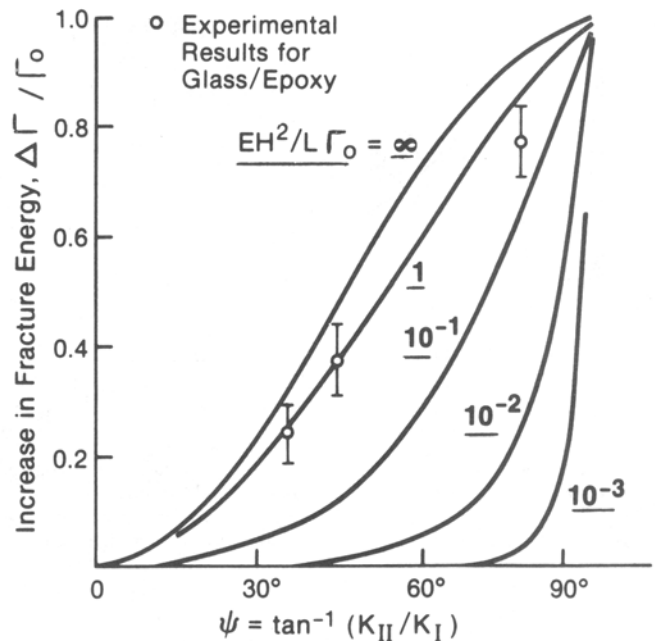


Fig. 15—Dislocations in the Nb around a Nb/Al₂O₃ bond.



(a)



(b)

Fig. 16—(a) Near tip schematic of the roughness-induced shielding model and (b) predictions of the model compared with experimental results for glass/polymer.

mechanics of elastic/plastic interface cracks. Nevertheless, some brief remarks are appropriate. *Crack shielding* by intact ligaments can be simply modeled^[35] based on observations of the plastic stretch of the ligaments, u_* , and the flow strength of the metal, Y , such that the increase in fracture energy is

$$\Delta\Gamma_i \cong fYu_* \quad [13]$$

where f is the area fraction of ligaments on the interface fracture surface. However, predictions of the interface conditions that give bridging and of the effects of the interface on the plastic stretch, which would be needed to understand this phenomenon, have yet to be attempted. Nevertheless, it is noted that u_* scales with $hY/E\Gamma_0$, giving the nondimensional parameter ζ expressed in Eq. [4].

Crack blunting by slip is another integral aspect of the

effect of plasticity. When blunting occurs, the crack tip stresses reduce to a small multiple of the metal flow stress.* Interface fracture would then seem to require ac-

*Analogy with homogeneous metals^[9] indicates that the peak stress should be of the order 3 to 6Y.

tivation of a brittle crack, whereupon the fracture energy may depend on near-interface flaws, as well as the flow stress of the metal. Finally, attention is drawn to the problem of whether an interface crack either blunts or remains sharp, an issue that relates to the paradox noted above for the Al₂O₃/Au interface. The problem involves both stationary cracks, which may blunt by dislocation ejection from the crack tip, and dynamic cracks, which can remain "sharp" when the viscoplastic properties of the metal exhibit high strain-rate sensitivity.^[10] Further study of these effects is clearly needed.

Finally, some brief remarks can be made concerning the crack path. In particular, reference to the Nb/Al₂O₃ system indicates that the crack remains at the interface, even though Γ_i is more than twice the fracture energy of the sapphire. An interpretation of this behavior is based upon recognition that ψ is negative (~ -5 deg), because the shear modulus for Nb is much smaller than that for Al₂O₃. Such negativity of ψ , as already noted, tends to trap the crack at the interface. Plastic deformation is thereby encouraged in the Nb, resulting in the relatively large Γ_i . However, the interface fracture mechanism involving such plasticity is not yet understood.

Another noteworthy feature of the Nb/Al₂O₃ system is that Γ_i is expected to diminish for rapidly moving interface cracks because of the strong rate sensitivity of plastic flow in Nb.^[33] Consequently, Γ_i may become smaller than the fracture energy of sapphire when the crack becomes unstable, further enforcing the preference for interface fracture.

VII. CONCLUDING REMARKS

Techniques for measuring the interface fracture energy over a wide range of phase angles now exist, as relevant to debonding problems of practical significance. Consequently, it is now possible to conduct a systematic study of trends in the fracture energy for a variety of interfaces and to develop models that relate $\Gamma_i(\psi)$ to microstructure. It is already apparent that Γ_i is typically much larger than the work of adhesion W_{ad} , indicating that extrinsic contributions to Γ_i must be sought and understood. Two contributions have been identified: roughness-induced shielding and plastic dissipation. The nondimensional parameters that govern these effects have been established, and their role in governing Γ_i for different interfaces has been afforded preliminary attention. Other components of Γ_i , such as reaction product layers, with associated residual strain, and segregation, also remain to be rigorously understood.

REFERENCES

1. A.G. Evans: *Mater. Sci. Eng.*, 1989, vol. A107, pp. 227-39.
2. A.G. Evans, M.Y. He, and J.W. Hutchinson: *J. Am. Ceram. Soc.*, 1989, vol. 72, pp. 2300-03.

3. K. Kendall: *J. Mater. Sci.*, 1976, vol. 11, pp. 638-41.
4. M.S. Hu and A.G. Evans: *Acta Metall.*, 1989, vol. 37, pp. 917-21.
5. Z. Suo and J.W. Hutchinson: *Mat. Sci. Eng.*, 1989, vol. A107, pp. 135-45.
6. A.G. Evans and J.W. Hutchinson: *Int. J. Solids Struct.*, 1984, vol. 20, pp. 455-61.
7. A.S. Argon, V. Gupta, H.S. Landis, and J.A. Cornie: *J. Mater. Sci.*, 1989, vol. A107, pp. 41-49.
8. H.C. Cao, M.D. Thouless, and A.G. Evans: *Acta Metall.*, 1988, vol. 36, pp. 2037-42.
9. B.J. Dalgleish, M.C. Lu, and A.G. Evans: *Acta Metall.*, 1988, vol. 36, pp. 2029-33.
10. J.R. Rice and J.S. Wang: *Mater. Sci. Eng.*, 1989, vol. A107, pp. 23-41.
11. R.M. Cannon, R.M. Fisher, and A.G. Evans: *MRS Proc.*, 1986, vol. 54, p. 799.
12. A.G. Evans and J.W. Hutchinson: *Acta Metall.*, 1989, vol. 37, pp. 909-15.
13. P.G. Charalambides: Michigan State University, East Lansing, MI, unpublished research, 1990.
14. J.W. Hutchinson: Harvard University, Cambridge, MA, unpublished research, 1990.
15. C.Y. Hui and H. Reidel: *Int. J. Fract.*, 1981, vol. 17, pp. 409-13.
16. M.Y. He and J.W. Hutchinson: *J. Appl. Mech.*, 1989, vol. 56, pp. 270-78.
17. J.R. Rice: *J. Appl. Mech.*, 1988, vol. 55, pp. 98-103.
18. M. Comninou and D. Schmueser: *J. Appl. Mech.*, 1979, vol. 46, pp. 345-47.
19. J.W. Hutchinson, M.E. Mear, and J.R. Rice: *J. Appl. Mech.*, 1987, vol. 109, pp. 828-30.
20. J. Dundurs: *Mathematical Theory of Dislocation*, ASME, New York, NY, 1969, p. 70.
21. T. Suga: Ph.D. Thesis, University of Stuttgart, Stuttgart, Federal Republic of Germany, 1984.
22. M.D. Thouless, A.G. Evans, M.F. Ashby, and J.W. Hutchinson: *Acta Metall.*, 1987, vol. 35, pp. 1333-40.
23. P. Matos, P.G. Charalambides, M.D. Drory, and R.M. McMeeking: *Int. J. Fract.*, in press.
24. P.G. Charalambides, J. Lund, R.M. McMeeking, and A.G. Evans: *J. Appl. Mech.*, 1989, vol. 111, pp. 77-82.
25. Z. Suo and J.W. Hutchinson: *Int. J. Fract.*, in press.
26. M.S. Hu, M.D. Thouless, and A.G. Evans: *Acta Metall.*, 1988, vol. 35, pp. 1301-06.
27. A.G. Evans, M.S. Hu, and M.D. Drory: *J. Mater.*, 1988, vol. 3, pp. 1043-50.
28. P.G. Charalambides and A.G. Evans: *J. Am. Ceram. Soc.*, 1989, vol. 72, p. 746.
29. M.Y. He, A. Bartlett, J. Hutchinson, and A.G. Evans: *J. Am. Ceram. Soc.*, in press.
30. K.S. Kim and N. Aravas: *Int. J. Solids Struct.*, 1988, vol. 24, pp. 417-22.
31. H.C. Cao and A.G. Evans: *Mech. Mater.*, 1989, vol. 7, pp. 295-304.
32. B.J. Dalgleish, K.P. Trumble, and A.G. Evans: *Acta Metall.*, 1989, vol. 37, pp. 1923-31.
33. M. Rühle and A.G. Evans: *MRS Proc.*, 1988, vol. 120, pp. 293-301.
34. P.G. Charalambides, H.C. Cao, J. Lund, and A.G. Evans: *Mech. Mtls.*, 1990, vol. 8, pp. 269-83.
35. T.S. Oh, J. Rodell, R.M. Cannon, and R.O. Ritchie: *Acta Metall.*, 1988, vol. 36, pp. 2083-90.
36. I. Reimanis, B.J. Dalgleish, M. Rühle, and A.G. Evans: *Acta Metall.*, in press.
37. W. Mader and M. Rühle: *Acta Metall.*, 1989, vol. 37, pp. 853-90.
38. A.G. Evans, M. Rühle, S. Schmauder, and M.C. Lu: *Acta Metall.*, 1986, vol. 34, pp. 1643-50.
39. R.M. McMeeking: *J. Mech. Phys. Solids*, 1977, vol. 25, pp. 357-63.
40. I. Reimanis and B.J. Dalgleish: University of California—Santa Barbara, unpublished research, 1988.